



Contents lists available at ScienceDirect

Journal of Geochemical Exploration

journal homepage: www.elsevier.com/locate/jgeoexp

Chemical compositions of garnet and clinopyroxene and their genetic significances in Yemaquan skarn iron–copper–zinc deposit, Qimantagh, eastern Kunlun

Pengfei Zuo ^a, Xuefei Liu ^{a,*}, Jinhua Hao ^b, Yashuai Wang ^a, Rui Zhao ^a, Songsheng Ge ^c^a State Key Laboratory of Geological Processes and Mineral Resources, China University of Geosciences, Beijing 100083, China^b Academy of Science, China University of Geosciences, Beijing 100083, China^c State Key Laboratory of Lithospheric Evolution, Institute of Geology and Geophysics, Chinese Academy of Sciences, Beijing 100029, China

ARTICLE INFO

Article history:

Received 28 December 2014

Revised 25 June 2015

Accepted 14 July 2015

Available online xxxx

Keywords:

Skarn iron–copper–zinc deposit

Prograde skarns

Skarn zonation

Mineralization zonation

Yemaquan

ABSTRACT

The Yemaquan skarn deposit in the northwestern part of the Qimantagh is located in the eastern Kunlun orogenic belt. The deposit is hosted in carbonate rocks, siltstones, and sandstones of the Cambrian–Ordovician Tanjianshan Group and Late Carboniferous Di’aosu Formation. These rocks are intruded by Triassic calc-alkaline granitoid that extended NW–SE. Three stages of mineralization have been identified, i.e., pre-ore stage, syn-ore stage, and post-ore stage. The prograde skarn stage, which corresponds to the pre-ore stage, is dominated by clinopyroxene and garnet. Clinopyroxene is much more abundant than garnet in the deposit and consists of three types of clinopyroxene in the deposit. In terms of the end-members diopside ($\text{CaMgSi}_2\text{O}_6$), hedenbergite ($\text{CaFeSi}_2\text{O}_6$), and johannsenite ($\text{CaMnSi}_2\text{O}_6$), namely, type I (with an average composition of $\text{Di}_{92}\text{Hd}_{7}\text{Joh}_{1}$), type II (with an average of composition of $\text{Di}_{62}\text{Hd}_{36}\text{Joh}_{2}$), and type III (with an average composition of $\text{Di}_{24}\text{Hd}_{54}\text{Joh}_{22}$) occurred from the proximal intrusions to the distal wall rocks. Type I, II, and III clinopyroxenes are associated with copper–iron, iron, and zinc–lead mineralization, respectively. Garnet mostly occurred in the middle of exoskarn zonations and is associated with type II clinopyroxene. The distribution of the garnet in the skarn zonation could be explained by the stability fields of clinopyroxene, which is strongly dependent on composition. Based on mineral assemblages, the formation of type II and type III, comparative to type I clinopyroxene, is in more reduced condition in the distal skarn. Moreover sulfur isotope carried out on sulfide minerals from both the prograde and retrograde stages show a variable and wide range of $\delta^{34}\text{S}$ values (−6.9 to 4.2‰ $\delta^{34}\text{S}$), suggesting that the skarn-forming fluid may have been affected by the reduced wall rocks. The low garnet/clinopyroxene ratios observed at the deposit might be caused by the clinopyroxene composition variations and reduced wall rocks.

© 2015 Elsevier B.V. All rights reserved.

1. Introduction

Skarn deposit zonation models based on the mineral assemblages have been widely used in mineral exploration. The development of a specific type of skarn depends on the local geological environment, such as the compositions of the sedimentary protolith and associated igneous rocks, depth of formation, and sulfur and oxygen fugacity (Cepedal et al., 2000; Ciobanu and Cook, 2004; Einaudi and Burt, 1982; Grammatikopoulos and Clark, 2006; Kamvong and Zaw, 2009; Lehrmann et al., 2009; Meinert, 1995; Meinert et al., 2005; Shimazaki, 1980). Although skarns cannot be solely characterized by their garnet or clinopyroxene compositions, consideration of both yields a relatively unique fingerprint, which serves as an additional aid in defining environments of formation (Gao et al., 2014a; Gaspar et al., 2008; Jamtveit and Hervig, 1994; Jamtveit et al., 1993, 1995; Liu et al., 2013; Smith

et al., 2004; Somarin, 2004; Zhai et al., 2013; Zhao, 1997; Zhao et al., 1997, 2002). Meinert (1992) and Meinert et al. (1997a, 2005) have discussed the relationship between the ratios of garnet/clinopyroxene and oxidation state within different skarn zonations.

The diopside, hedenbergite, and johannsenite are typical clinopyroxene in iron, copper, and lead–zinc skarn deposits, respectively and are widely utilized to study the ore-forming processes and ore exploration, especially johannsenite, which commonly develops far from intrusions (e.g., Bonev et al., 2005; Bussell et al., 1990; Canet et al., 2009; Einaudi et al., 1981; Einaudi and Burt, 1982; Mao et al., 1996; Meinert, 1982, 1987; Palinkaš et al., 2013; Zhao et al., 1983, 2002) and has been studied by many researchers (Abrecht, 1980; Angel, 1984; Burt, 1977; Capitani et al., 2003; Dimanov and Sautter, 2000; Vassileva and Bonev, 2001, 2002, 2003).

The Qimantagh in the eastern Kunlun orogenic belt is one of the most important Fe–Cu resource bases in China. Most of the ore deposits are concealed skarn deposits that have been geologically researched very little. Mn-, Fe-, and Mg-rich skarn deposits, including Yemaquan, Galinge, Sijiaoyang, and Kendekeke deposits, are developed widely in

* Corresponding author.

E-mail address: lxf@cugb.edu.cn (X. Liu).

the district. The Yemaquan Fe–Cu–Zn deposit in the Qimantagh is one typical representative of the skarn deposits in this area (Liu et al., 2013; Zhang, 2012; Zhao et al., 2013). The geological features of both intrusions and skarns, ages of intrusions and metallogenic epoch, origin of the deposits, and the metallogenic setting have been comprehensively investigated (Feng et al., 2010, 2011a; Gao et al., 2014b; Liu et al., 2013; Song et al., 2010; Wang et al., 2009; Zhang, 2012; Zhao et al., 2013). However, the low ratios of garnet/clinopyroxene and their links to the mineralization are still obscure. In this paper, a comprehensive petrographic, mineralogical, and sulfur isotope study of the skarns developed at different spatial positions relative to the intrusions were conducted with the aim of gaining a better understanding of the skarn and mineralization zonations in the Qimantagh.

2. Regional geology

The eastern Kunlun orogenic belt lies on the northern Tibetan Plateau with the Songpan–Garzê accretionary complex to the south and Qaidam Basin to the north. It can be subdivided into three tectonic zones according to the major faults: North, Middle, and South Kunlun Fault (Fig. 1a) (Jiang et al., 1992; Li et al., 2013a; Meng et al., 2013, 2015; Xia et al., 2014; Xu et al., 2014; Yang et al., 1996). The Qimantagh district is located in the northwestern part of the North Zone.

The Precambrian basement in the Qimantagh is mainly composed of Paleoproterozoic to Neoproterozoic medium- to high-grade metamorphic rocks, carbonate formations, and meta-clastic rocks (Jiang et al., 1992; Wang et al., 2010, 2012). It was overlain by the Tanjianshan Group, Cambrian to Ordovician in age, which includes shallow and

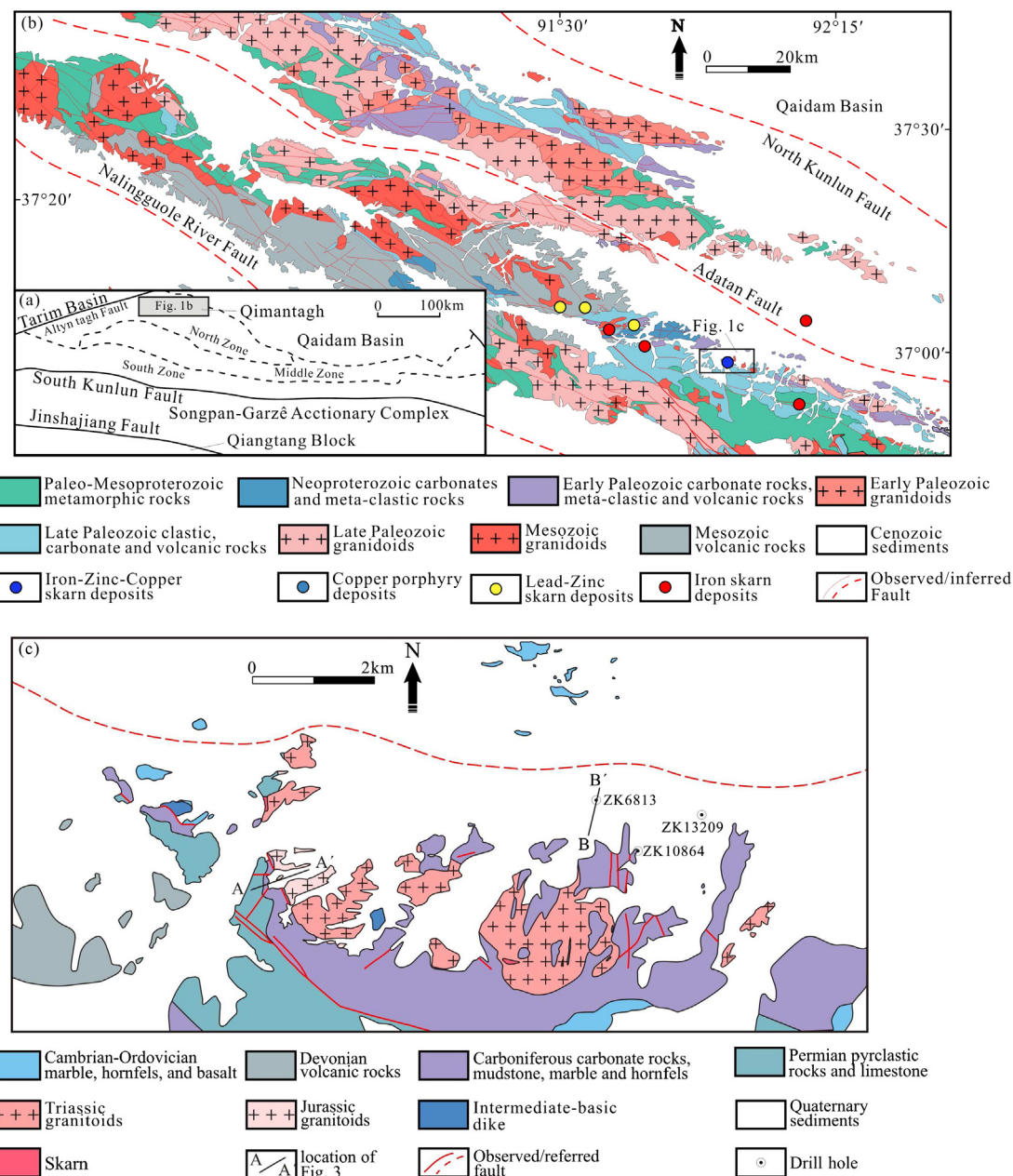


Fig. 1. (a) Schematic map showing the three sub-tectonic zones of the eastern Kunlun orogenic belt (after Jiang et al., 1992; Xu et al., 1996; Deng et al., 2012, 2013, 2014a, 2015a). (b) Geologic map of the Qimantagh area (modified from geologic maps of the Qimantagh district by QGSI, 2009; locations of the North, Adatan and Nalingguole River fault based on Wang et al., 2009, 2012, and Wang, 2011). (c) Geologic map of the Yemaquan iron–copper–zinc deposit (modified from a geologic map of the Yemaquan deposit by TEIGMRQ, 2010).

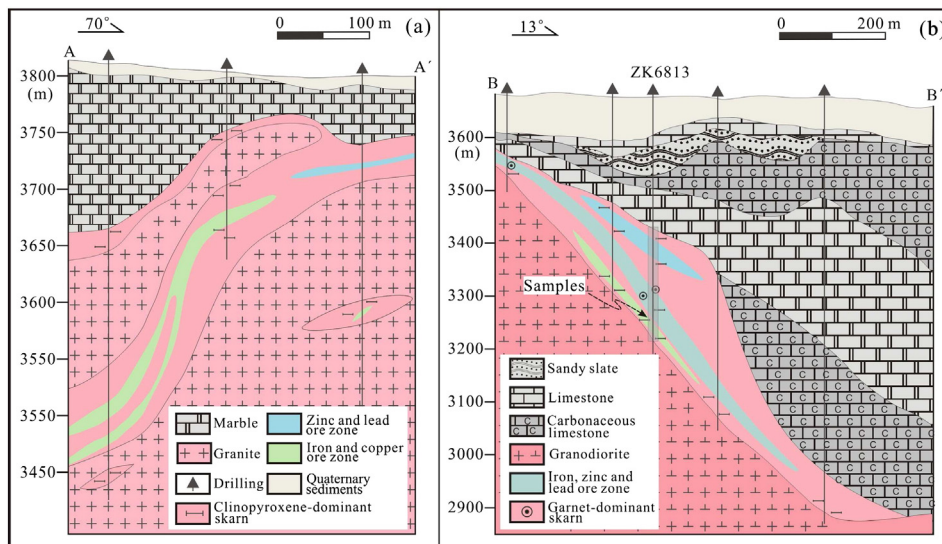


Fig. 2. Geologic cross sections through the Yemaquan iron–copper–zinc deposit, show the spatial relationship among different strata units, intrusions, skarn and orebodies, based on TEIGMRQ (2010). See Fig. 1d for locations. (a) Iron–copper and zinc–lead ore zone associated with the granite in endoskarn. (b) The mineralization zone from copper–iron to zinc–lead mineralization with distal to granodiorite. The location of samples in ZK6813.

deep-water clastics, carbonate rocks, volcanic rocks, and volcanic clastic rocks (Jiang et al., 1992; Pan et al., 1996; Wang et al., 2010, 2012; Yin and Harrison, 2000; Yin and Zhang, 1997). A molasse formation deposited from Late Silurian to Early Devonian indicated the closure of the Qimantagh Ocean (Proto-Tethys Ocean) (Pan et al., 1996; Jiang et al., 2000; Hao et al., 2014; Wang et al., 2014; Li et al., 2015a; Li et al., 2015b; Xiong et al., 2015; Hao et al., 2015). Carboniferous marine sedimentary rocks (Di'aosu Formation) of the active continental margin developed in the district (Chen et al., 2006; Feng et al., 2011a; Jiang et al., 1992; Li et al., 2008; Zhang et al., 2004).

Magmatism was very active in the Early Paleozoic (518–420 Ma) and related with the northward subduction of the Qimantagh Ocean (Cui et al., 2011; Li et al., 2013a; Meng et al., 2013, 2015). Accretion/collision magmatism developed from the start of the Late Silurian (~406 Ma–~350 Ma) and indicated that this district formed part of the collisional orogeny stage (Chen et al., 2006; Li et al., 2013a; Liu et al., 2012). From the Permian to Middle Triassic, abundant granitoids (280 Ma–250 Ma) intruded during this period and were associated with the Paleo-Tethys oceanic basin subducting northward (Deng et al., 2014b; Huang et al., 2014; Li et al., 2001, 2013a, 2013b; Mo et al., 2007; QRGST, 1981; Xiong et al., 2013; Yang et al., 1996). The granitoids of Middle Triassic to Early Jurassic (230–190 Ma) indicated the closure of the Paleo-Tethys Ocean and the Eastern Kunlun area entered the intracontinental orogenic stage (Deng et al., 2015b; Guo et al., 1998;

Kui et al., 2010; Li et al., 2015c; Mo et al., 2007; Li et al., 2015d; Ding et al., 2015; Hu et al., 2015; Wang et al., 2016). A great number of skarn-type and porphyry-related poly-metallic deposits are temporally and spatially related to Middle to Late Triassic granitic intrusions (235–219 Ma) (Fig. 1b) (Chang et al., 2009; Feng et al., 2011a, 2011b, 2012; Gao et al., 2012; Li et al., 2008; Liu et al., 2006; She et al., 2007; Xi et al., 2010; Xiao et al., 2013; Zhao et al., 2013).

3. Geology of the Yemaquan deposit

Based on outcrops and drill cores (Figs. 1c and 2), the strata at Yemaquan mainly consists of the Tanjianshan Group of Cambrian and Ordovician, the Maoniushan Formation of Late Devonian, the Di'aosu Formation of Late Carboniferous, and the Dachaigou Formation of Early and Middle Permian. Ore-bearing strata are dominated by the limestone in the Tanjianshan Group and the Di'aosu Formation (Xiao et al., 2013; Zhang, 2012). The Tanjianshan Group consists of granoblastic- to hypautomorphic-marble, chert, and lepidogranoblastic hornfels interbedded with basalt. The Di'aosu Formation can be divided into three parts from the bottom to the top, based on TEIGMRQ (2010), i.e., (1) skarn and silicated limestone; (2) hornfels, quartz sandstone, silty mudstone, siltstone, greywacke, and breccia; (3) marble and carbonaceous limestone. Small granodiorite and syenogranite intrusions (Fig. 3a, b) and other neutral or felsic rocks were emplaced during the

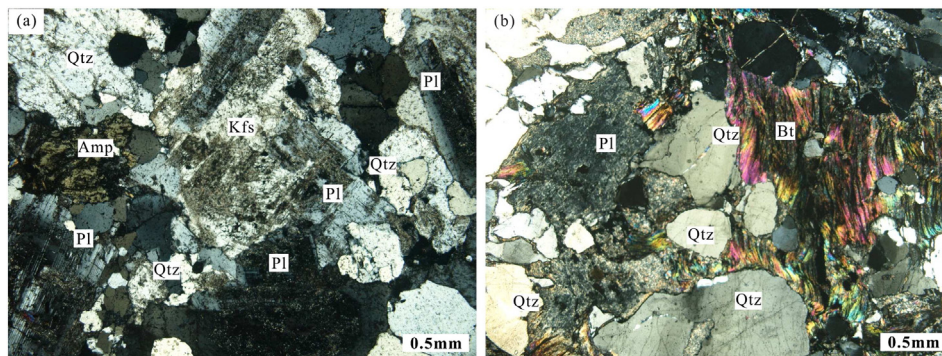


Fig. 3. Photomicrographs of intrusive rocks in the Yemaquan Fe–Zn deposit: (a) granodiorite, polysynthetic twin of plagioclase and simple twin of albited alkali feldspar; (b) syenogranite, carbonatization and kaolinization of plagioclase and chloritization of biotite. Mineral abbreviations: Amp—amphibole; Pl—plagioclase; Bt—biotite; Qtz—quartz; Kfs—alkali feldspar.

intense magmatism period from the Late Triassic to Early Jurassic (Feng et al., 2010, 2011a; Gao et al., 2014b). LA-ICP-MS U-Pb zircon dating reveals that the biotite diorite, quartz adamellite, and syenogranite at Yemaquan were emplaced at 220.0 ± 0.45 Ma, 223.3 ± 0.54 Ma, and 213 ± 1.0 Ma, respectively (Gao et al., 2014b; Zhang, 2012).

Prominent faults strike NWW, N-E, and N-W, representing favorable sites for mineralization (TEIGMRQ, 2010). The locations of the orebodies generally run parallel to the bedding of the host rocks (Fig. 2). It is hard to find fresh granitoid rocks within the deposit, most of them having been chloritized, silicified, albited, and/or kaolinized (Fig. 3). The skarns developed along the contact zones between the main intrusion and the marble, siliceous limestone, silty limestone, and carbonaceous limestone. The major ore types are Fe-, Zn-, and Cu-bearing skarns. Unambiguously, the mineralization zonations of Fe, Cu within the deposit are proximal to the intrusions, whereas those for Zn, Pb occur far from the intrusions (Fig. 2). In the Yemaquan skarn deposit, clinopyroxene is widely developed in both the proximal and the distal parts of the skarn, but garnet is less abundant and mostly

occurs in the middle part of the skarn zone (Figs. 2 and 4) (TEIGMRQ, 2010). The skarn zonation is different from most skarn deposits, which have a general spatial zonation pattern ranging from endoskarn alteration within the causative intrusion, proximal garnet, distal clinopyroxene at the contact between skarn and marble (Einaudi and Burt, 1982; Meinert et al., 1997a, 2005).

4. Sampling and analytical methods

Sixty-six skarn samples of the drill cores of ZK6813 (42 samples), ZK13209 (13 samples) and ZK10864 (6 samples), were collected consecutively from the intrusive body to wall rocks. These samples were cut into thin, polished sections in the laboratory of China University of Geosciences (Beijing) and used for textural and mineral paragenetic sequence studies. Nineteen of them were analyzed for mineral composition and six samples in the ZK6813 drill core for sulfur isotope analyses (for locations, see Fig. 4a) in the State Key Laboratory of GPMR, China University of Geosciences (Beijing).

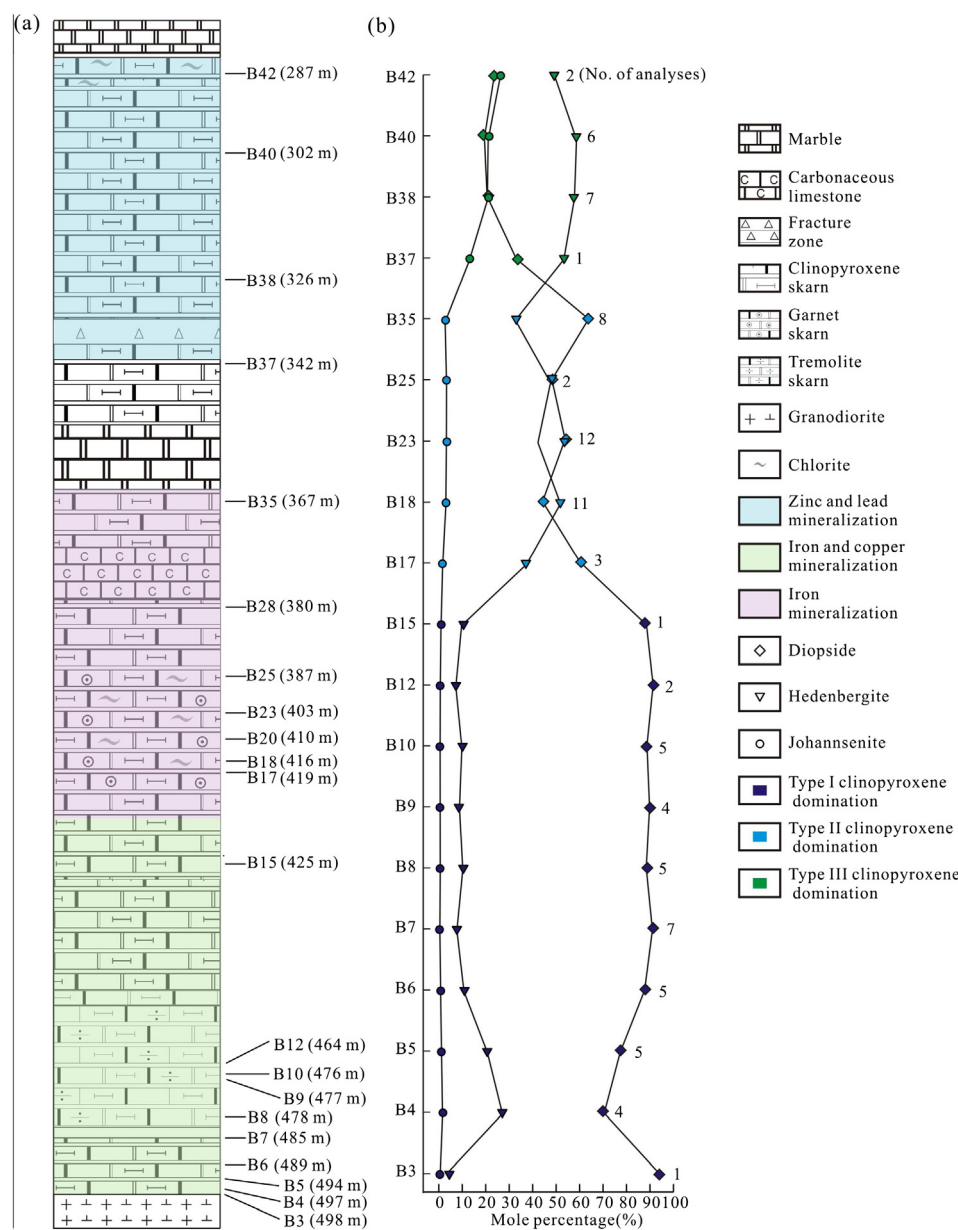


Fig. 4. (a) Schematic column showing the zonation of skarns and mineralization in no. ZK6813 diamond drill core. (b) Average mole percentage of clinopyroxene end members in the drilling core (ZK6813).

Minerals	Pre-ore stage	Syn-ore stage	Post-ore stage
Clinopyroxene			
Garnet			
Wollastonite			
Magnetite			
Pyrite			
Chalcopyrite			
Pyrrhotite			
Quartz			
Calcite			
Amphibole			
Apatite			
Sphalerite			
Galena			
Scheelite			
Chlorite			
Fluorite			
Serpentine			
Sericite			
Hematite			
Limonite			

Fig. 5. Mineral paragenesis for the Yemaquan iron–copper–zinc deposit.

In order to investigate the formation of the prograde skarn, several points were analyzed on a single grain of clinopyroxene and garnet using an electron microprobe (EPMA-1600). Wavelength dispersive spectrometry (WDS) analyses were carried out at the following conditions: for silicates: 15 kV, 10 nA, beam diameter of 1 μm , and a counting time of 30 s. Detected limits in terms of weight percent oxides for the elements in these analyses are estimated as follows: SiO_2 , Al_2O_3 , MgO , K_2O , Na_2O –0.05 wt.%; CaO –0.04 wt.%; and, TiO_2 , Cr_2O_3 , FeO , MnO , and ZnO –0.03 wt.%. The chemical formulae of garnet and clinopyroxene were obtained using the method of oxygen atom calculation (Zheng, 1983), and the ratios of Fe^{2+} and Fe^{3+} of clinopyroxene and garnet were obtained on the basis of the balance of electrovalence. Corrections for matrix effects were applied according to procedures described by Bence and Albee (1968) and Albee and Ray (1970).

The sulfur isotope analysis procedure has been described by Robinson and Kusakabe (1975) and was performed with an EA-IRISPRIME100. Sulfur isotope ratios are reported as $\delta^{34}\text{S}$ relative to the Vienna-Canyon Diablo Troilite (V-CDT). The analytical precision for $\delta^{34}\text{S}$ is $\leq 0.15\text{\%}$.

5. Mineral paragenetic sequence

The prograde minerals are predominantly clinopyroxene and garnet. Small amounts of wollastonite, chalcopyrite, magnetite, and pyrrhotite

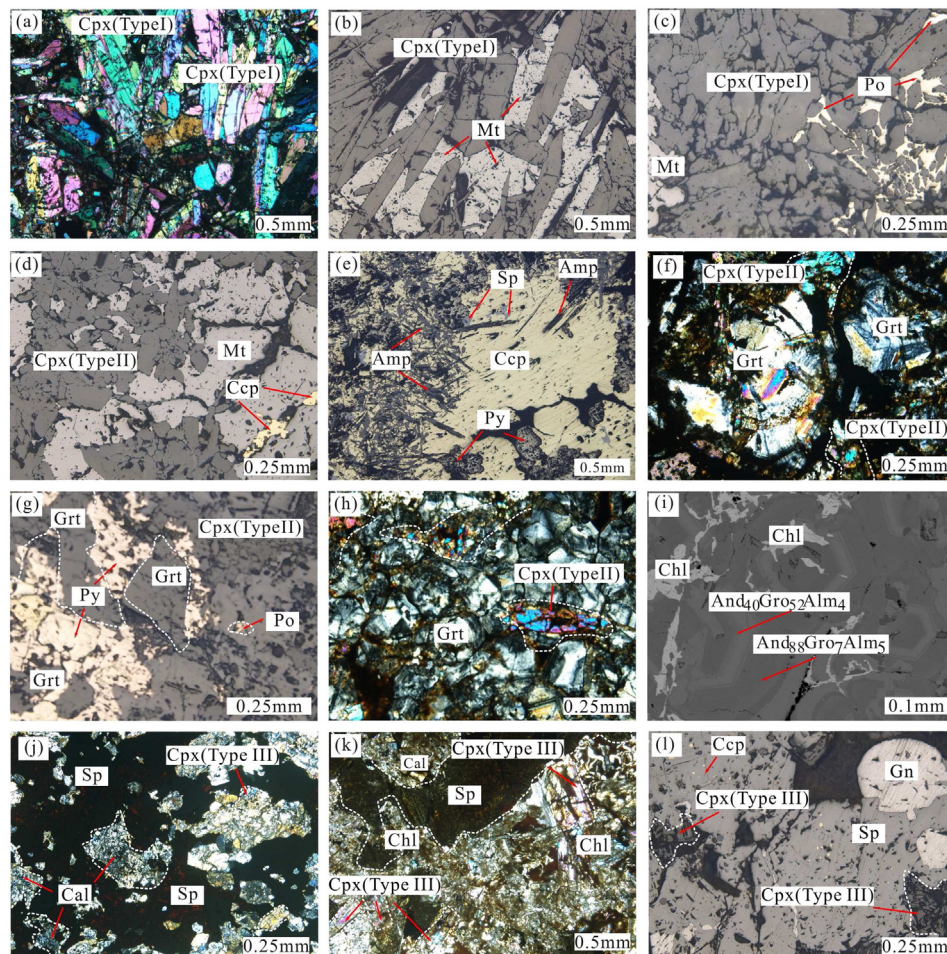


Fig. 6. Photomicrographs of sample at the Yemaquan Fe–Zn deposit. (a) and (b) Coarse, bladed diopsidic (Type I) clinopyroxene with interstitial magnetite. Sample B6. (c) Coarse, bladed clinopyroxene with interstitial pyrrhotite and metasomatic magnetite. Sample B9. (d) Clinopyroxene associated with metasomatic magnetite and pyrite. Sample B10. (e) Needle amphibole associated with chalcopyrite, sphalerite and pyrite. Sample B12. (f) and (g) Garnet replaced clinopyroxene (Type II). Coarse-grained and zoned garnet with pyrite and pyrrhotite (g, Type II garnet). Sample B17. (h) Saccharoidal garnet replaced clinopyroxene (Type II) and various degrees of selective replacement of garnet by chlorite (i). The replacement mostly occurs along certain bands of garnet, whereas some occurs as veins cutting across the bands (BSE). Sample B23. (j) Type III clinopyroxene associated with sphalerite. Sample B37. (k) Calcite and chlorite replaced clinopyroxene (Type III). Galena occurs as vein within sphalerite (l). Sample B42. Abbreviations: Mt—magnetite; Po—pyrrhotite; Cpx—clinopyroxene; Ccp—chalcopyrite; Sp—sphalerite; Py—pyrite; Grt—garnet; And—andalusite; Gro—grossular; Alm—almandine; Chl—chlorite; Cal—calcite; Gn—galena.

Table 1

Electron microprobe analyses of skarn clinopyroxenes (wt.%).

Sample	B3-1	B4-1	B4-2	B5-1	B5-2	B5-3	B6-1	B6-2	B7-1	B7-2	B8-1	B8-2	B9-1	B9-2	B10-1
Number	1	2	2	2	2	1	2	3	5	2	2	3	2	2	3
Type	I	I	II	II	I	I	II	I	I	I	I	II	I	I	I
<i>Weight percentage</i>															
SiO ₂	54.51	54.28	51.48	52.25	54.45	54.84	53.15	54.81	54.68	53.80	54.65	53.10	53.72	54.71	54.63
TiO ₂	0.07	0.09	n.d.	0.12	0.04	0.05	0.06	n.d.	0.04	n.d.	n.d.	0.11	0.04	0.12	0.04
Al ₂ O ₃	n.d.	n.d.	0.11	0.88	n.d.	0.05	0.21	0.21	0.26	0.13	n.d.	0.41	0.18	n.d.	0.09
FeO*	2.28	4.26	15.61	14.66	2.36	4.38	8.15	2.22	2.60	5.77	2.45	6.84	5.65	2.58	2.27
MnO	0.25	0.30	0.84	0.62	0.21	0.51	0.59	0.14	0.17	0.32	0.07	0.39	0.39	0.11	0.18
MgO	17.88	16.88	9.56	9.84	17.88	16.67	14.24	18.13	17.79	16.07	18.26	15.45	16.03	17.99	17.89
CaO	24.36	24.17	22.52	21.34	24.56	24.50	23.52	24.46	24.46	23.99	24.44	23.68	23.95	24.46	24.36
Na ₂ O	0.07	0.07	0.04	0.14	0.07	n.d.	0.15	0.06	0.06	n.d.	0.07	0.07	0.05	0.06	n.d.
K ₂ O	n.d.	n.d.	n.d.	0.03	n.d.	n.d.	n.d.	n.d.	n.d.	n.d.	n.d.	n.d.	n.d.	n.d.	n.d.
Total	99.42	100.04	100.14	99.86	99.56	101.00	100.06	100.03	100.06	100.06	99.93	100.05	100.00	100.02	99.46
<i>Citations based on 6 oxygens</i>															
Si	1.99	1.99	1.99	2.00	1.99	1.99	1.99	1.99	1.99	1.99	1.99	1.97	1.98	1.99	1.99
Al	0.00	0.00	0.04	0.00	0.00	0.00	0.00	0.00	0.01	0.00	0.00	0.00	0.00	0.00	0.00
Ti	0.00	0.00	0.00	0.00	0.00	0.00	0.00	0.00	0.00	0.00	0.00	0.00	0.00	0.00	0.00
Fe ³⁺	0.02	0.03	0.03	0.04	0.03	0.01	0.04	0.02	0.02	0.04	0.04	0.06	0.04	0.03	0.01
Fe ²⁺	0.05	0.10	0.47	0.44	0.04	0.12	0.21	0.05	0.06	0.14	0.03	0.16	0.13	0.05	0.06
Mn	0.01	0.01	0.03	0.02	0.01	0.02	0.02	0.00	0.01	0.01	0.00	0.01	0.01	0.00	0.01
Mg	0.97	0.92	0.55	0.56	0.97	0.90	0.79	0.98	0.96	0.88	0.99	0.85	0.88	0.98	0.97
Ca	0.95	0.95	0.93	0.88	0.96	0.95	0.94	0.95	0.95	0.95	0.95	0.94	0.95	0.95	0.95
Na	0.00	0.00	0.00	0.01	0.00	0.00	0.01	0.00	0.00	0.00	0.00	0.00	0.00	0.00	0.00
K	0.00	0.00	0.00	0.00	0.00	0.00	0.00	0.00	0.00	0.00	0.00	0.00	0.00	0.00	0.00
Total	4.01	4.01	4.01	3.98	4.01	4.00	4.01	4.00	4.01	4.01	4.01	4.00	4.01	4.01	4.00
<i>Mole percentage</i>															
Joh	0.75	0.90	2.62	1.97	0.64	1.51	1.81	0.42	0.50	0.95	0.20	1.20	1.18	0.33	0.54
Di	94.56	89.43	52.40	55.22	95.58	87.06	77.49	95.17	93.81	85.53	96.54	83.61	85.74	94.74	94.01
Hd	4.69	9.67	44.98	42.80	3.79	11.43	20.70	4.41	5.68	13.51	3.26	15.18	13.08	4.94	5.45

Note: n.d. = not detected; FeO* = total iron content; Joh=johannsenite, Di=diopside, and Hd=hedenbergite.

developed. The early retrograde skarn consists of amphibole, quartz, and the metallic minerals, with minor fluorite, serpentine, chlorite, apatite, and calcite. A final stage of retrograde alteration is characterized by calcite, quartz, sericite, hematite, and chlorite. The main metallic minerals are magnetite, sphalerite, galena, pyrite, chalcopyrite, and pyrrhotite. Based on previous studies (e.g., Li et al., 2013a; Song et al., 2010; Zhang, 2012) and our petrographic investigations, three stages of ore deposition during skarnization have been identified. The later stage commonly partially replaced earlier stages. The paragenetic sequence is illustrated in Fig. 5. These three stages are (1) pre-ore stage (clinopyroxene–garnet–magnetite–chalcopyrite–pyrrhotite ± wollastonite); (2) syn-ore stage (sulfides–magnetite–amphibole–quartz–calcite–scheelite ± garnet ± clinopyroxene); and (3) post-ore stage (calcite–chlorite–quartz–fluorite).

5.1. Pre-ore stage

Similar to many skarn systems, prograde minerals like clinopyroxene and garnet in this stage represent the earliest skarn-forming phase. Based on characteristics of mineral assemblages and structures, three types of clinopyroxene have been identified. Type I clinopyroxene is about 0.5 mm across, platy or flaky, much bigger than type II and III, and is associated with magnetite, chalcopyrite and pyrrhotite (Fig. 6a, b, and c). Magnetite fills interstices of clinopyroxene with straight fringes and occurs as isolated banding (Fig. 6b), while pyrrhotite is also interstitial within the clinopyroxene (Fig. 6c). By contrast, Type II and type III clinopyroxenes are subhedral to anhedral (Fig. 6f, h, j, and k). Type II clinopyroxene is typically associated with garnet, magnetite, pyrite, pyrrhotite, and minor chalcopyrite (Fig. 6d, f, g, and h). Type III clinopyroxene is commonly associated with sphalerite and galena (Fig. 6j, k and l).

Two types of garnet also developed. Type I garnet is very small (ca. 10–20 µm), not associated with clinopyroxene, and without zoning,

and may be formed by early metamorphism in which the calc-silicate hornfels developed (Meinert et al., 2005). Type II garnet in the deposit is generally fine in size (ca. 0.25 mm) (Fig. 6f and h), euhedral to subhedral, and replaced clinopyroxene (Fig. 6f and h). The garnets are colorless to light tan in thin section and typically display anomalous birefringence with sector zoning. They are commonly rimmed and replaced by later chlorite (Fig. 6i).

5.2. Syn-ore stage

Syn-ore stage is characterized by the frequent occurrence of metasomatic sulfides, magnetite, and minor scheelite (Fig. 5). Retrograde minerals in this stage coexisting with these sulfides mainly include quartz, calcic amphiboles, calcite, and chlorite with lesser garnet. Amphibole is often difficult to distinguish in hand specimen, but it appears as radiating clusters under the microscope and is associated with sphalerite and chalcopyrite mineralization (Fig. 6e). Sulfides in the Yemaquan deposit include sphalerite, galena, chalcopyrite, pyrite, and pyrrhotite. Other sulfides documented in previous publications at the deposit are bismuthinite, bornite, tetrahedrite, and lillianite (Zhang, 2012). Generally, sphalerite, galena, chalcopyrite, pyrite, and magnetite in this stage are associated with type II clinopyroxene. The Cu–Fe → Fe → Zn–Pb mineralization zone is shown in Fig. 4a. The ore minerals commonly cut the skarn minerals and/or filled up the interstices between them. It is clear, therefore, that ore deposition in this stage occurred later than the precipitation of the clinopyroxene.

5.3. Post-ore stage

During the post-ore stage, only some low-temperature alteration minerals were formed. Among them, calcite is dominant, with minor limonite, hematite, quartz, sericite, serpentine, chlorite, apatite, and

B10-2	B12-1	B12-2	B15-1	B17-1	B18-1	B23-1	B25-1	B25-2	B35-1	B35-2	B37-1	B38-1	B40-1	B40-2	B42-1	B42-2
2	1	1	1	3	11	12	1	1	2	6	1	7	3	3	1	1
II	I	I	I	II	II	II	II	II	II	III	III	III	III	III	III	III
53.45	53.82	55.14	54.62	51.77	50.75	51.24	51.24	49.34	52.73	51.78	49.85	49.05	49.41	49.18	49.54	49.79
0.08	n.d.	0.04	n.d.	n.d.	0.05	0.03	0.20	n.d.	0.03	0.03	n.d.	0.06	0.05	n.d.	n.d.	n.d.
0.60	0.08	n.d.	n.d.	0.24	0.14	n.d.	0.57	0.19	0.21	0.30	0.17	0.31	0.26	0.37	0.13	n.d.
6.46	5.39	1.42	3.99	13.63	17.69	15.44	12.56	22.79	8.96	12.95	17.24	19.02	17.02	21.16	20.76	12.13
0.34	0.41	0.13	0.38	0.58	0.98	1.10	0.60	1.72	0.85	0.94	4.02	6.23	7.30	4.68	6.02	9.97
15.13	15.99	18.54	17.02	10.90	7.87	9.79	13.38	5.24	13.70	10.92	5.83	3.57	4.15	2.91	2.57	5.74
23.91	24.21	24.84	24.29	22.81	22.47	22.32	20.99	20.06	23.49	22.91	21.92	21.45	21.55	21.45	21.86	22.02
0.10	0.07	n.d.	n.d.	0.14	0.11	0.07	n.d.	n.d.	0.06	0.11	0.08	0.20	0.21	0.16	0.06	0.11
n.d.	n.d.	n.d.	n.d.	n.d.	n.d.	n.d.	n.d.	n.d.	n.d.	n.d.	n.d.	n.d.	n.d.	n.d.	n.d.	n.d.
100.05	99.97	100.11	100.30	100.06	100.06	99.98	99.54	99.34	100.02	99.94	99.11	99.89	99.96	99.89	100.94	99.76
1.98	1.99	1.99	1.99	1.98	1.99	1.98	1.96	1.99	1.98	1.98	1.99	1.98	1.99	1.99	1.99	1.98
0.03	0.00	0.00	0.00	0.00	0.00	0.00	0.01	0.00	0.00	0.01	0.01	0.01	0.01	0.02	0.00	0.00
0.00	0.00	0.00	0.00	0.00	0.00	0.00	0.01	0.00	0.00	0.00	0.00	0.00	0.00	0.00	0.00	0.00
0.03	0.04	0.02	0.02	0.05	0.04	0.05	0.08	0.02	0.05	0.04	0.02	0.05	0.05	0.01	0.02	0.05
0.17	0.13	0.03	0.10	0.39	0.53	0.44	0.32	0.75	0.23	0.37	0.56	0.59	0.53	0.70	0.68	0.35
0.01	0.01	0.00	0.01	0.02	0.03	0.04	0.02	0.06	0.03	0.03	0.14	0.21	0.25	0.16	0.21	0.34
0.83	0.88	1.00	0.93	0.62	0.46	0.56	0.76	0.31	0.77	0.62	0.35	0.21	0.25	0.17	0.15	0.34
0.95	0.96	0.96	0.95	0.94	0.94	0.93	0.86	0.87	0.95	0.94	0.94	0.93	0.93	0.94	0.94	0.94
0.01	0.01	0.00	0.00	0.01	0.01	0.01	0.00	0.00	0.01	0.01	0.02	0.02	0.01	0.00	0.01	0.01
0.00	0.00	0.00	0.00	0.00	0.00	0.00	0.00	0.00	0.00	0.00	0.00	0.00	0.00	0.00	0.00	0.00
4.01	4.01	4.01	4.01	4.01	4.01	4.01	4.00	4.00	4.01	4.01	4.01	4.01	4.01	4.00	4.00	4.01
1.05	1.26	0.39	1.13	1.83	3.19	3.44	1.76	5.24	2.63	2.95	13.08	20.90	24.35	18.13	19.72	32.82
82.08	86.38	97.06	88.94	60.60	44.70	54.05	69.15	28.08	74.93	60.71	33.39	21.00	24.16	15.20	14.81	33.26
16.88	12.37	2.56	9.93	37.57	52.11	42.51	29.09	66.68	22.44	36.33	53.53	58.10	51.48	66.67	65.47	33.92

fluorite. These minerals occur as veinlets crosscutting skarns and sulfides.

6. Analytical results

6.1. Chemical compositions of garnet and clinopyroxene

EPMA results of the clinopyroxene and garnet from the deposit are listed in [Tables 1 and 2](#). The compositions of the clinopyroxene are expressed in terms of mole fractions of the three end members, i.e., hedenbergite (Hd), johannsenite (Joh), and diopside (Di) as there is no miscibility gap between hedenbergite–diopside on one side and johannsenite on the other ([Abrecht, 1985](#)). The chemical data of all analyzed clinopyroxenes are plotted together and cluster into three different areas within the diopside–hedenbergite–johannsenite ternary plot ([Fig. 7a](#)). Type I clinopyroxene falls in the Cu–Fe range, type II in the Fe range and type III in the Zn range.

The more manganese-rich clinopyroxene formed from fluids, which are distal in the overall zonation sequence ([Di et al., 2006; Gemmell et al., 1992; Meinert, 1987; Zhao et al., 2003](#)). In contrast, clinopyroxene formed in proximal locations is rich in magnesium and iron ([Fig. 4b](#)). The chemical compositions of the three types of clinopyroxene show the correlation, which is consistent with our observation under the microscope. Based on BSE images and EPMA data, type I and II clinopyroxenes generally occur with exsolved Fe-rich clinopyroxene as banding (5–10 µm in width). Type III clinopyroxene consists of iron-rich terms at the center and grade to manganese-rich terms towards the rim. In general, clinopyroxenes found in ore-bearing skarn tend to be enriched in iron and manganese, whereas those in barren skarn are enriched in magnesium. These features indicate that iron and manganese concentrated in the ore bodies, were already enriched in the fluid during skarn formation ([Shimizu and Iiyama, 1982](#)).

Compared with clinopyroxene, garnet shows less regular iron enrichment. [Fig. 7b](#) shows the ternary proportion of its grossular–andradite–pyralspite, and the relationships with the Cu, Fe and Zn skarn deposits worldwide. Type I garnet ($\text{And}_{<6}\text{Gro}_{>88}\text{Alm}_{<5}$) not associated with mineralization is poikilitic. Overall, type II garnet forms an essentially andradite–grossular solid solution from $\text{And}_{40}\text{Gro}_{55}\text{Alm}_5$ to $\text{And}_{90}\text{Gro}_3\text{Alm}_6$, with spessartine and pyrope less than 7 and 2 mol%, and fills the area of Zn, Fe and Cu skarn deposits. Generally, type II garnet replaced type II clinopyroxene and is associated with iron mineralization ([Fig. 6f, g and h](#)).

6.2. Sulfur isotopes

Sulfur isotope compositions of pyrite, chalcopyrite, pyrrhotite, sphalerite, and galena from the ores are listed in [Table 3](#) and are associated with both prograde and retrograde skarn. The $\delta^{34}\text{S}$ values for sulfides vary from -6.9 to $+4.2\text{\textperthousand}$. The chalcopyrite sample of the prograde skarn stage has $\delta^{34}\text{S}$ value of $4.2\text{\textperthousand}$. While the other samples, i.e., pyrite, pyrrhotite, and sphalerite, are from the retrograde skarn stage. One pyrite sample has a $\delta^{34}\text{S}$ value of $-6.9\text{\textperthousand}$ and two other pyrite samples have $\delta^{34}\text{S}$ values of 1.8 and $2.6\text{\textperthousand}$. The sphalerite and pyrrhotite have $\delta^{34}\text{S}$ values of 3.2 and $2.8\text{\textperthousand}$. Based on these results, there is evidence that these samples become more depleted in ^{34}S content as the distance from the intrusive body increases.

7. Discussion

The skarn zonation is controlled by temperature, depth of formation, fluid/rock ratios, compositions and oxidation state of associated intrusions and wall rocks ([Chowdhury and Lentz, 2011; Deng et al., 2011, 2014c; Fuertes-Fuente et al., 2000; Kuçcu et al., 2002; Levresse and Gonzalez-Partida, 2003; Meinert et al., 2005; Oyman, 2010; Pons et al., 2010; Scheepers, 2000; Somarin and Moayyed, 2002; Williams-Jones](#)

Table 2

Electron microprobe analyses of skarn garnets (wt.%).

Sample no.	B17-1	B17-2	B18-1	B18-2	B18-3	B18-4	B23-1	B23-2	B23-3	B23-4
Number	2	1	4	6	2	3	7	3	5	1
Type	II	II	I	II	II	II	II	II	II	II
<i>Weight percentage</i>										
SiO ₂	37.59	38.03	40.15	38.37	39.10	37.34	38.22	38.54	37.14	37.70
TiO ₂	0.07	0.00	0.58	0.42	0.16	1.04	0.30	0.07	0.04	0.00
Al ₂ O ₃	4.29	12.52	20.85	10.12	11.92	7.51	10.18	12.23	2.34	3.87
FeO*	25.11	14.94	2.69	17.70	15.80	20.46	17.99	15.60	27.64	25.63
MnO	0.46	0.98	0.08	1.05	0.94	2.08	1.08	1.16	0.48	0.52
MgO	0.28	0.05	0.23	n.d.	0.05	n.d.	n.d.	n.d.	0.09	0.07
CaO	31.40	31.74	34.22	32.11	32.33	31.48	31.98	32.39	32.00	32.24
Total	99.18	98.26	98.80	99.76	100.29	99.92	99.74	100.00	99.72	100.03
<i>Citations based on 12 oxygens</i>										
Si	3.05	3.03	3.05	3.03	3.05	2.99	3.03	3.02	3.03	3.04
Ti	0.00	0.00	0.03	0.02	0.01	0.06	0.02	0.00	0.00	0.00
Al	0.41	1.18	1.87	0.94	1.10	0.71	0.95	1.13	0.22	0.37
Fe ³⁺	1.55	0.81	0.07	1.02	0.86	1.26	1.02	0.85	1.75	1.60
Fe ²⁺	0.15	0.19	0.10	0.15	0.17	0.11	0.17	0.17	0.13	0.13
Mn	0.03	0.07	0.01	0.07	0.06	0.14	0.07	0.08	0.03	0.04
Mg	0.03	0.01	0.03	0.00	0.01	0.00	0.00	0.00	0.01	0.01
Ca	2.73	2.71	2.79	2.72	2.70	2.70	2.71	2.72	2.80	2.79
Total	7.96	7.98	7.94	7.96	7.96	7.97	7.97	7.98	7.98	7.97
<i>Mole percentage</i>										
And	79.11	40.66	3.85	51.93	44.04	64.00	51.81	42.94	88.64	81.33
Pyr	1.15	0.20	0.88	0.00	0.20	0.00	0.00	0.00	0.36	0.28
Spe	1.06	2.23	0.18	2.38	2.10	4.79	2.46	2.59	1.11	1.20
Gro	13.58	50.52	91.79	40.52	47.93	27.47	39.98	48.66	5.51	12.92
Alm	5.10	6.39	3.29	5.17	5.73	3.75	5.76	5.81	4.38	4.26

Note: And—andalite, Gro—grossular, Alm—almandine, Pyr—pyrope, Spe—spessartine.

et al., 2010). The garnet/clinopyroxene ratios can give important clues about these fundamental geological variables, serve as a crude indicator of the general oxidation state of the system, and be applied to both the classification and exploration of the skarn deposits (Einaudi, 1981; Gaspar et al., 2008; Logan, 2000; Lu et al., 2003; Meinert et al., 1997b; Öztürk and Helvaci, 2008; Somarin, 2004).

7.1. Physicochemical conditions of prograde skarn formation

Based on the uplift and exhumation studies in the district, the depth of formation of the Yemaquan deposit was at 7 km and the pressure was roughly 2 kb (Wang et al., 2003; Yuan et al., 2006). The relatively deep environment is consistent with field observations such as the absence of brecciation and brittle fracture associated with mineralization, widely developed calc-silicate hornfels, and the intrusive contacts subparallel to bedding (Meinert et al., 2005). Conditions for the Mt-Po-Py invariant point fixed at 550 °C with a log f_{S_2} value of −3.25 and $\log f_{\text{O}_2}$ value

of −18.7 (Fig. 8; Ciobanu and Cook, 2004). The upper f_{O_2} limit is considered to lie below the Hu/Mt buffer, based on the absence of hematite. Type I clinopyroxene in association with the magnetite has a magmatic affiliation (Fig. 6b) (Zharikov, 1970), including MgO contents of up to 3 wt.%. In addition, the upper limit temperature of the magmatic magnetite in equilibrium with type I clinopyroxene is estimated to be 650 °C, (Ciobanu and Cook, 2004). The absence of wollastonite that associated with type I clinopyroxene indicates $X(\text{CO}_2) < 0.1$ (Greenwood, 1967) (Fig. 8). Andradite stability in f_{O_2} - f_{S_2} space is temperature dependent: below 600 °C, andradite is stable with Py; whereas from 500 to 300 °C, andradite is stable with Py plus magnetite (Gamble, 1982). Due to the lack of more complete experimental data on clinopyroxene solid solutions, it is not possible to offer the stability fields of type II ($\text{Di}_{62}\text{Hd}_{36}\text{Joh}_{2}$) and type III ($\text{Di}_{24}\text{Hd}_{54}\text{Joh}_{22}$) clinopyroxenes. However, as pointed out by Gamble (1982) and Burton (1982), manganese is far more effective than magnesium at expanding the clinopyroxene stability field. Gamble (1982) showed that at 2 kb, $\text{Di}_{75}\text{Hd}_{25}$ coexisting with

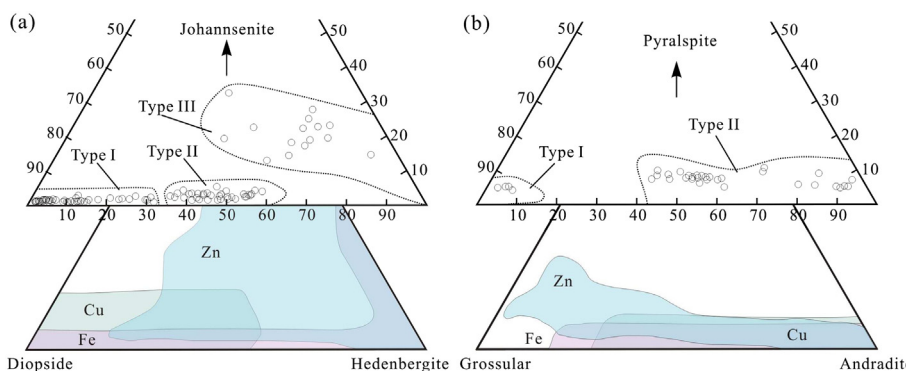


Fig. 7. Ternary diagrams summarizing clinopyroxene (a) and garnet compositions at the Yemaquan iron–copper–zinc deposit (b). Colored areas indicate the clinopyroxene and garnet composition ranges for zinc, iron and copper skarn deposits summarized by Meinert (1992). Pyrospite = (pyrope + almandine + spessartine). (For interpretation of the references to color in this figure legend, the reader is referred to the web version of this article.)

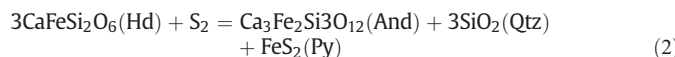
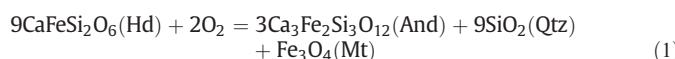
Table 3

Sulfur isotopic compositions from the Yemaquan iron–copper–zinc deposit.

Sample no.	Drill core and depth	Mineral	Skarn stage	$\delta^{34}\text{S}_{\text{V}-\text{CDT}}\%$
B4	ZK6813, 497 m	Chalcopyrite	Prograde skarn stage	4.19
B15	ZK6813, 425 m	Pyrite	Retrograde skarn stage	2.59
B20	ZK6813, 410 m	Pyrrhotite	Retrograde skarn stage	2.81
B23	ZK6813, 403 m	Pyrite	Retrograde skarn stage	1.76
B28	ZK6813, 380 m	Pyrite	Retrograde skarn stage	−6.88
B35	ZK6813, 367 m	Sphalerite	Retrograde skarn stage	3.19

Py is stable only below 550 °C and Hd₅₀Di₅₀ coexisting with Py below 395 °C. Therefore, the upper temperature limit for type II and type III clinopyroxenes is estimated to be 550 °C.

The garnet occurred in the middle of exoskarn zonation and was mainly associated with iron mineralization. This could be explained by the replacement of diopside–hedenbergite by pyrite, pyrrhotite, magnetite, and andradite, which show the change in the system leading to garnet, magnetite and iron sulfides deposition (Fig. 6g, h, and i) according to reactions (1) and (2) (Burton et al., 1982):



7.2. The formation of prograde skarn and ore

As pointed out by Dimanove and Wiedenbeck (2006), the (Fe, Mn)–Mg interdiffusion coefficient is strongly $f\text{O}_2$ sensitive. More oxidizing conditions would favor the formation of andradite and diopsidic clinopyroxene relative to hedenbergite (Gamble, 1982; Gustafson, 1974). Furthermore, Gro-rich garnet (type II garnet, with an average composition of And₆₁Gro₃₂Spe₂Alm₅), is a garnet that requires lower $f\text{O}_2$ than an And-rich equivalent (Einaudi and Burt, 1982). The clinopyroxene enrichment sequence Mg–Fe–Mn is interpreted as resulting largely from fluid depletion and temperature decrease (Capitani and Mellini, 2000; Meinert, 1987). For this reason, the probable path of prograde skarn

formation has been shown in Fig. 8. The formation of type II and type III, comparative to type I clinopyroxene, therefore occurs attained in more reducing conditions in the distal skarn.

The wide range of $\delta^{34}\text{S}$ values for all sulfides and the decrease in $\delta^{34}\text{S}$ values in distal skarns suggest that the ore minerals might have been deposited as a result of the decrease in the oxidation state and temperature further from intrusions (Fu et al., 1991). Furthermore, the widespread occurrence of the carbonaceous limestone has also led to abnormal disturbance in electrical prospecting (TEIGMRQ, 2010). In spite of the fact that the sulfides postdate the skarn, a systematic correlation exists between specific prograde skarn mineral compositions and the presence of ore. This means that the ore-forming process was controlled in some way by the clinopyroxene skarn itself (Shimizu and Iiyama, 1982). Therefore, the tendency of the estimated physicochemical environment during prograde skarn formation might also suggest the principal causes of ore formation are a reduction of the ore-forming fluid and a decrease in temperature. Furthermore, in reactions (1) and (2), the formation of magnetite and pyrite could also have been caused by the replacement of type II clinopyroxene. This is consistent with the fact type II clinopyroxene is mainly associated with iron mineralization.

8. Conclusion

- Compared to type I clinopyroxene, the formation of type II and III clinopyroxenes took place in more reducing conditions in the distal skarn. The low ratios of garnet/clinopyroxene in the deposit are caused by the compositions of clinopyroxene and the reduced wall rocks. The garnet, which is less abundant than the clinopyroxene, could have been produced by a progressive reduction of the mineralizing fluids as a result of their interaction with the organic matter of the carbonaceous limestone.
- Type I, II, and III clinopyroxenes are associated with copper–iron, iron, and zinc–lead mineralization, respectively. The tendency of the estimated physicochemical environment during prograde skarn formation might also suggest the principal causes of ore formation are a reduction of the ore-forming fluid and a decrease in temperature.
- An increase in hedenbergite and johannsenite and a decrease in the diopside content of clinopyroxene are observed through the deposit sequence Cu–Fe → Fe → Zn–Pb. Such associations could be used to identify skarn zonations and be useful in future exploration in this district.

Acknowledgments

We are grateful to Senior Engineers Dongsheng Li, Aikui Zhang, and other technical staff in the Third Exploration Institute of Geology and Mineral Resources of Qinghai, for their support during the fieldwork. Many thanks are extended to Prof. Jianping Chen, Dehui Zhang, and Dr. Xiaobo Zhao and Yaoyao Zhang. All of them have greatly assisted me with their constructive suggestions. We gratefully acknowledge the constructive reviews from Dr. Yi Cao, Martin-Izard, and two anonymous journal reviewers. This research was jointly supported by the

Fig. 8. Log $f\text{O}_2$ –temperature diagram for Hd and Hd₈₅Joh₁₅ oxidation reaction. Mineral stability fields on the basis of experimental data from Moehler and Chou (1990), and Burton et al. (1982). Magnetite–hematite based on Haas and Robie (1973). The position of the calc–silicate equilibrium reaction: Cal + Qtz → Wo + CO₂ is shown assuming an X(CO₂) = 0.2 and 0.1, considering a decrease in this parameter from proximal to distal settings (data presented by Greenwood, 1967). Hm + Cal + Qz → And is at X(CO₂) = 0.03 (data presented by Bowman, 1998, in Ciobanu and Cook, 2004). The position of Py/Mt, Py/Po, Mt/Po, Cp/Bn + Mt, and Cp/Bn + po from data presented for by Simon et al. (2000).

National Basic Research Program (Nos. 2015CB452600) and the National Natural Science Foundation of China (No. 41202061 and 41302043).

References

- Abrecht, J., 1980. Stability relations in the system CaSiO_3 – $\text{CaMnSi}_2\text{O}_6$ – $\text{CaFeSi}_2\text{O}_6$. *Contrib. Mineral. Petrol.* 74, 253–260.
- Abrecht, J., 1985. Manganiferous pyroxenes and pyroxenoids from three Pb–Zn–Cu skarn deposits. *Contrib. Mineral. Petrol.* 89, 379–393.
- Albee, A.L., Ray, L., 1970. Correction factors for electron probe microanalysis of silicates, oxides, carbonates, phosphates, and sulfates. *Anal. Chem.* 42, 1408–1414.
- Angel, R.J., 1984. The experimental determination of the johannsenite–bustamite equilibrium inversion boundary. *Contrib. Mineral. Petrol.* 85, 272–278.
- Bence, A.E., Albee, A.L., 1968. Empirical correction factors for the electron microanalysis of silicates and oxides. *J. Geol.* 76, 382–403.
- Bonev, I.K., Vassileva, R.D., Zотов, N., Kouzmanov, K., 2005. Manganilvate, $\text{CaFe}^{2+}\text{Fe}^{3+}(\text{Mn}, \text{Fe}^{2+})_2\text{Si}_2\text{O}_7\text{O(OH)}$, a new mineral of the group from skarn deposits in the Rhodope Mountains, Bulgaria. *Can. Mineral.* 43, 1027–1042.
- Burt, D.M., 1977. Mineralogy and petrology of skarn deposits. *Soc. Italiana Mineralogia Petrologia Rend.* 33, 859–873.
- Burton, J.C., Taylor, L.A., Chou, I.M., 1982. The f_{O_2} -T and f_{S_2} -T stability relations of hedenbergite and of hedenbergite–johannsenite solid solutions. *Econ. Geol.* 77, 764–783.
- Bussell, M.A., Alpers, C.N., Petersen, U., Shepherd, T.J., Bermudez, C., Baxter, A.N., 1990. The Ag–Mn–Pb–Zn vein, replacement, and skarn deposits of Uchucchacua, Peru; studies of structure, mineralogy, metal zoning, Sr isotopes, and fluid inclusions. *Econ. Geol.* 85, 1348–1383.
- Canet, C., Camprubí, A., González-Partida, E., Linares, C., Alfonso, P., Piñeiro-Fernández, F., Prol-Ledesma, R.M., 2009. Mineral assemblages of the Francisco I. Madero Zn–Cu–Pb–(Ag) deposit, Zacatecas, Mexico: implications for ore deposit genesis. *Ore Geol. Rev.* 35, 423–435.
- Capitaní, G.C., Mellini, M., 2000. The johannsenite–hedenbergite complete solid solution clinopyroxenes from the Campiglia Marittima skarn. *Eur. J. Mineral.* 12, 1215–1227.
- Capitaní, G.C., Grobety, H.B., Mellini, M., 2003. Reaction sequences, polysomatic faults and chemical compositions of manganese pyroxenoids. *Eur. J. Mineral.* 15, 381–391.
- Cepedal, A., Martín-Izard, A., Reguilón, R., Rodríguez-Pévida, L., Spiering, E., González-Nistal, S., 2000. Origin and evolution of the calcic and magnesian skarns hosting the El Valle-Boinás copper–gold deposit, Asturias (Spain). *J. Geochem. Explor.* 71 (2), 119–151.
- Chang, Y.Y., Li, J.F., Zhang, J., Cao, S.X., Li, P.P., Chen, H.Q., 2009. Study of environment and chronology of Late Triassic intrusive rocks in east Nalinggele river of Qinghai-Northeast. *Econ. Geol.* 42 (1), 57–65 (in Chinese with English abstract).
- Chen, H.W., Luo, Z.H., Mo, X.X., Zhang, X.T., Wang, J., Wang, B.Z., 2006. SHRIMP ages of Keyakedengtage complex in the East Kunlun Mountains and their geological implications. *Acta Petrol. Mineral.* 25, 25–32 (in Chinese with English abstract).
- Chowdhury, S., Lentz, D.R., 2011. Mineralogical and geochemical characteristics of scheelite-bearing skarns, and genetic relations between skarn mineralization and petrogenesis of the associated granitoid pluton at Sargipali, Sundergarh District, Eastern India. *J. Geochem. Explor.* 108, 39–61.
- Ciobanu, C.L., Cook, N.J., 2004. Skarn textures and a case study: the Ocna de Fier-Dognecea orefield, Banat, Romania. *Ore Geol. Rev.* 24 (3), 315–370.
- Cui, M.H., Meng, F.C., Wu, X.K., 2011. Early Ordovician island arc of Qimantag Mountain, eastern Kunlun: evidences from geochemistry, Sm–Nd isotope and geochronology of intermediate–basic igneous rocks. *Acta Petrol. Sin.* 27 (11), 3365–3379 (in Chinese with English abstract).
- Deng, J., Wang, Q.F., Xiao, C.H., Yang, L.Q., Liu, H., Gong, Q.J., Zhang, J., 2011. Tectonic–magmatic–metallogenic system, Tongling ore cluster region, Anhui Province, China. *Int. Geol. Rev.* 53, 449–476.
- Deng, J., Wang, C.M., Li, G.J., 2012. Style and process of the superimposed mineralization in the Sanjiang Tethys. *Acta Petrol. Sin.* 28, 1349–1361 (in Chinese with English abstract).
- Deng, J., Ge, L.S., Yang, L.Q., 2013. Tectonic dynamic system and compound orogeny: additionally discussing the temporal–spatial evolution of Sanjiang orogeny, Southwest China. *Acta Petrol. Sin.* 29, 1099–1114 (in Chinese with English abstract).
- Deng, J., Wang, C.M., Santosh, M., 2014a. Orogenesis and metallogenesis in the Sanjiang Tethyan domain, China: preface. *Gondwana Res.* 26, 415–418.
- Deng, J., Wang, Q.F., Li, G.J., Li, C.S., Wang, C.M., 2014b. Tethys tectonic evolution and its bearing on the distribution of important mineral deposits in the Sanjiang region, SW China. *Gondwana Res.* 26, 419–437.
- Deng, J., Wang, Q.F., Li, G.J., Santosh, M., 2014c. Cenozoic tectono-magmatic and metallogenic processes in the Sanjiang region, southwestern China. *Earth-Sci. Rev.* 138, 268–299.
- Deng, J., Wang, Q.F., Li, G.J., Zhao, Y., 2015a. Structural control and genesis of the Oligocene Zhanyuan orogenic gold deposit, SW China. *Ore Geol. Rev.* 65, 42–54.
- Deng, J., Wang, Q.F., Li, G.J., Hou, Z.Q., Jiang, C.Z., Danyushevsky, L., 2015b. Geology and genesis of the giant Beiya porphyry–skarn gold deposit, northwestern Yangtze Block, China. *Ore Geol. Rev.* 70, 457–485.
- Di, Y.J., Wu, G.G., Zhang, D., Yu, X.Q., Lin, D.Y., Shi, J.J., Zang, W.S., Zhang, X.X., Wang, Q.F., 2006. Composition characteristics of pyroxenes from Pb–Zn deposits in central Fujian Province and their genetic significance. *Mineral Deposits* 25, 123–134 (in Chinese with English abstract).
- Dimanov, A., Sautter, V., 2000. "Average" interdiffusion of (Fe, Mn)–Mg in natural diopside. *Eur. J. Mineral.* 12, 749–760.
- Dimanov, A., Wiedenbeck, M., 2006. (Fe, Mn)–Mg interdiffusion in natural diopside: effect of $p\text{O}_2$. *Eur. J. Mineral.* 18, 705–718.
- Ding, Q.F., Liu, F., Yan, W., 2015. Zircon U–Pb geochronology and Hf isotopic constraints on the petrogenesis of Early Triassic granites in the Wulonggou area of the Eastern Kunlun Orogen, Northwest China. *Int. Geol. Rev.* 57 (13), 1735–1754.
- Einaudi, M.T., Burt, D.M., 1982. Introduction—terminology, classification, and composition of skarn deposits. *Econ. Geol.* 77, 745–754.
- Einaudi, M.T., Meinert, L.D., Newberry, R.J., 1981. Skarn deposits. *Society of Economic Geologists, Economic Geology 75th Anniversary Volume* pp. 317–391.
- Feng, C.Y., Zhang, D.Q., Li, D.S., Sun, Y., Li, G.C., Ma, S.C., 2010. Metallogenetic regularity study of Qimantage, Qinghai. *Mineral Deposits* 29, 3–4 (in Chinese with English abstract).
- Feng, C.Y., Zhao, Y.M., Li, D.X., Liu, J.N., Xiao, Y., Li, G.C., Ma, S.C., 2011a. Skarn types and mineralogical characteristics of the Fe–Cu–polymetallic skarn deposits in the Qimantage Area, Western Qinghai Province. *Acta Geol. Sin.* 85, 1108–1115 (in Chinese with English abstract).
- Feng, C.Y., Wang, X.P., Shu, X.F., Zhang, A.K., Liu, J.N., Ma, S.C., Li, G.C., Li, D.X., 2011b. Isotopic chronology of the Houtuya skarn lead–zinc polymetallic ore district in Qimantage area of Qinghai Province and its geological significance. *J. Jilin Univ.: Earth Sci.* 6, 1806–1817 (in Chinese with English abstract).
- Feng, C.Y., Wang, S., Li, G.C., Ma, S.C., Li, D.S., 2012. Middle to Late Triassic granitoids in the Qimantage area, Qinghai Province, China: chronology, geochemistry and metallogenetic significances. *Acta Petrol. Sin.* 28 (2), 665–678 (in Chinese with English abstract).
- Fu, M., Changkakoti, A., Krouse, H.R., Gray, J., Kwak, T.A.P., 1991. An oxygen, hydrogen, sulfur, and carbon isotope study of carbonate-replacement (skarn) tin deposits of the Dachang tin field, China. *Econ. Geol.* 86 (8), 1683–1703.
- Fuertes-Fuente, M., Martin-Izard, A., Nieto, J.G., Maldonado, C., Varela, A., 2000. Preliminary mineralogical and petrological study of the Ortosa Au–Bi–Te ore deposit: a reduced gold skarn in the northern part of the Rio Narcea Gold Belt, Asturias, Spain. *J. Geochem. Explor.* 71, 177–190.
- Gamble, R.P., 1982. An experimental study of sulfidation reactions involving andradite and hedenbergite. *Econ. Geol.* 77, 784–797.
- Gao, Y.B., Li, W.Y., Ma, X.G., Zhang, Z.W., Tang, Q.Y., 2012. Genesis, geochronology and Hf isotopic compositions of the magmatic rocks in Galinge iron deposit, eastern Kunlun. *J. Lanzhou Univ. (Nat. Sci.)* 48, 36–47 (in Chinese with English abstract).
- Gao, X., Deng, J., Meng, J.Y., Yan, H., Li, J.X., Yang, C.H., Sun, N., Wei, C., 2014a. Characteristics of garnet in the Hongnian skarn copper deposit, western Yunnan. *Acta Petrol. Sin.* 30 (9), 2695–2708 (in Chinese with English abstract).
- Gao, Y.B., Li, W.Y., Qian, B., Li, D.S., He, S.Y., Zhang, Z.W., Zhang, J.W., 2014b. Geochronology, geochemistry and Hf isotopic compositions of the granitic rocks related with iron mineralization in Yemaquan deposit, East Kunlun, NW China. *Acta Petrol. Sin.* 30, 1647–1665 (in Chinese with English abstract).
- Gaspar, M., Knaack, C., Meinert, L.D., Moretti, R., 2008. REE in skarn systems: a LA-ICP-MS study of garnets from the Crown Jewel gold deposit. *Geochim. Cosmochim. Acta* 72 (1), 185–205.
- Gemmell, J.B., Zantop, H., Meinert, L.D., 1992. Genesis of the Aguilar zinc–lead–silver deposit, Argentina: contact metasomatic vs. sedimentary exhalative. *Econ. Geol.* 87, 2085–2112.
- Grammatikopoulos, T.A., Clark, A.H., 2006. A comparative study of wollastonite skarn genesis in the Central Metasedimentary Belt, southeastern Ontario, Canada. *Ore Geol. Rev.* 29 (2), 146–161.
- Greenwood, H.J., 1967. Wollastonite: Stability in H_2O – CO_2 mixtures and occurrence in a contact–metamorphic aureole near Salmo, British Columbia, Canada. *Am. Mineral.* 52, 1669–1680.
- Guo, Z.F., Deng, J.F., Xu, Z.Q., Mo, X.X., Luo, Z.H., 1998. Late Paleozoic–Mesozoic intercontinental orogenic process and intermediate-acidic igneous rocks from the Eastern Kunlun Mountains of Northwestern China. *Geoscience* 12, 344–352 (in Chinese with English abstract).
- Gustafson, W.I., 1974. The stability of andradite, hedenbergite, and related minerals in the system Ca–Fe–Si–O–H. *J. Petrol.* 15 (3), 455–496.
- Haas, J.L., Robie, R.A., 1973. Thermodynamic data for wustite, $\text{Fe}_{0.947}\text{O}$ magnetite, Fe_3O_4 , and hematite, Fe_2O_3 . *Am. Geophys. Union Trans.* 54, 488.
- Hao, N.N., Yuan, W.M., Zhang, A.K., Cao, J.H., Chen, X.N., Feng, Y.L., Li, X., 2014. Late Silurian to Early Devonian granitoids in the Qimantag Area, East Kunlun Mountains: LA-ICP-MS zircon U–Pb ages, geochemical features and geological setting. *Geol. Rev.* 60, 201–215 (in Chinese with English abstract).
- Hao, N.N., Yuan, W.M., Zhang, A.K., Feng, Y.L., Cao, J.H., Chen, X.N., Cheng, X.Q., Mo, X.X., 2015. Evolution process of the Late Silurian–Late Devonian tectonic environment in Qimantag in the western portion of east Kunlun, China: evidence from the geochronology and geochemistry of granitoids. *J. Earth Syst. Sci.* 124 (1), 171–196.
- Hu, Y., Niu, Y.L., Li, J.Y., Ye, L., Kong, J.J., Chen, S., Zhang, Y., Zhang, G.R., 2015. Petrogenesis and tectonic significance of the Late Triassic mafic dikes and felsic volcanic rocks in the East Kunlun Orogenic Belt, Northern Tibet Plateau. *Lithos*. <http://dx.doi.org/10.1016/j.lithos.2015.05.004>.
- Huang, H., Niu, Y., Nowell, G., Zhao, Z., Yu, X., Zhu, D.C., Mo, X.X., Ding, S., 2014. Geochemical constraints on the petrogenesis of granitoids in the East Kunlun Orogenic belt, northern Tibetan Plateau: implications for continental crust growth through syn-collisional felsic magmatism. *Chem. Geol.* 370, 1–18.
- Jamtveit, B., Hervig, R.L., 1994. Constraints on transport and kinetics in hydrothermal systems from zoned garnet crystals. *Science* 263 (5146), 505–507.
- Jamtveit, B., Wogelius, R.A., Fraster, D.G., 1993. Zonation patterns of skarn garnets—records of hydrothermal system evolution. *Geology* 21 (2), 113–116.
- Jamtveit, B., Ragnarsdóttir, K.V., Wood, B.J., 1995. On the origin of zoned grossular–andradite garnets in hydrothermal systems. *Eur. J. Mineral.* 7, 1399–1410.
- Jiang, C.F., Yang, J.S., Feng, B.G., Zhu, Z.Z., Zhao, M., Chai, Y., Shi, X.D., Wang, H.D., Hu, J.Q., 1992. Opening–Closing Tectonics of Kunlun Mountains. *Geol. Pub. House, Beijing*, pp. 1–224 (in Chinese with English abstract).

- Jiang, C.F., Wang, Z.Q., Li, J.Y., 2000. Opening–Closing Tectonics of Central Orogenic Belt. *Geol. Pub. House, Beijing*, pp. 1–154 (in Chinese).
- Kamvong, T., Zaw, K., 2009. The origin and evolution of skarn-forming fluids from the Phu Lon deposit, northern Loei Fold Belt, Thailand: evidence from fluid inclusion and sulfur isotope studies. *J. Asian Earth Sci.* 34 (5), 624–633.
- Kui, M.J., Bai, H.X., Gu, F.B., Miao, G.W., 2010. Division of East Kunlun tectonic magmatic belt and the rock tectonic combination in the late Variscan–Yanshanian period. *J. Qinghai Univ. (Nat. Sci.)* 28, 49–55 (in Chinese with English abstract).
- Kuşcu, I., Gençlioğlu Kuşcu, G., Meinert, L.D., Floyd, P.A., 2002. Tectonic setting and petrogenesis of the Çelebi granitoid, (Kirikkale-Turkey) and comparison with world skarn granitoids. *J. Geochem. Explor.* 76 (3), 175–194.
- Lehrmann, B., Oliver, N.H., Rubenach, M.J., Georges, C., 2009. The association between skarn mineralisation and granite bodies in the Chillagoe region, North Queensland, Australia. *J. Geochem. Explor.* 101 (1), 58.
- Levresse, G., Gonzalez-Partida, E., 2003. Highly oxidised gold skarn fluids evolution in the Mezcalo deposit, Guerrero, Mexico. *J. Geochem. Explor.* 78–79, 649–652.
- Li, G.M., Shen, Y.C., Liu, T.B., 2001. Geological and geochemical characteristics of Variscan granite in the Qimantagh region, Eastern Kunlun. *Geol. Pros.* 37, 73–78 (in Chinese with English abstract).
- Li, S.J., Sun, F.Y., Feng, C.Y., Liu, Z.H., Zhao, J.W., Li, Y.C., Wang, S., 2008. Geochronological study on Yazigou polymetallic deposit in eastern Kunlun, Qinhai Province. *Acta Geol. Sin.* 82 (7), 949–955 (in Chinese with English abstract).
- Li, W., Neubauer, F., Liu, Y., Genser, J., Ren, S., Han, G., Liang, C., 2013a. Paleozoic evolution of the Qimantagh magmatic arcs, Eastern Kunlun Mountains: constraints from zircon dating of granitoids and modern river sands. *J. Asian Earth Sci.* 77, 183–202.
- Li, G.J., Wang, Q.F., Yu, L., Hu, Z.C., Ma, N., Huang, Y.H., 2013b. Closure of the Ailaoshan Paleo-Tethys ocean: constraints by the zircon U-Pb dating and geochemistry of the late Permian granitoids. *Acta Petrol. Sin.* 29, 3883–3900 (in Chinese with English abstract).
- Li, C.S., Zhang, Z.W., Li, W.Y., Wang, Y.L., Sun, T., Ripley, E.M., 2015a. Geochronology, petrology and Hf-S isotope geochemistry of the newly-discovered Xiarihamu magmatic Ni–Cu sulfide deposit in the Qinghai–Tibet plateau, western China. *Lithos* 216, 224–240.
- Li, R.B., Pei, X.Z., Li, Z.C., Pei, L., Liu, C.J., Chen, Y.X., Chen, G.C., Liu, Z.Q., Yang, J., 2015b. Geochemistry and zircon U-Pb geochronology of granitic rocks in the Buqingshan tectonic mélange belt, northern Tibet Plateau, China and its implications for Prototethyan evolution. *J. Asian Earth Sci.* 105, 374–389.
- Li, G.J., Deng, J., Wang, Q.F., Liang, K., 2015c. Metallogenetic model for the Laochang Pb-Zn-Ag–Cu volcanogenic massive sulfide deposit related to a Paleo-Tethys OIB-like volcanic center, SW China. *Ore Geol. Rev.* 70, 578–594.
- Li, X.W., Huang, X.F., Luo, M.F., Dong, G.C., Mo, X.X., 2015d. Petrogenesis and geodynamic implications of the Mid-Triassic lavas from East Kunlun, northern Tibetan Plateau. *J. Asian Earth Sci.* 105, 32–47.
- Liu, Y.H., Mo, X.X., Yu, X.H., Zhang, X.T., Xu, G.W., 2006. Zircon SHRIMP U-Pb dating of the Jingren granite, Yemaquan region of the east Kunlun and its geological significance. *Acta Petrol. Sin.* 22, 2457–2463 (in Chinese with English abstract).
- Liu, B., Ma, C.Q., Zhang, J.Y., Xiong, F.H., Huang, J., Jiang, H.A., 2012. Petrogenesis of Early Devonian intrusive rocks in the east part of Eastern Kunlun Orogen and implication for Early Palaeozoic orogenetic processes. *Acta Petrol. Sin.* 28 (6), 1785–1807 (in Chinese with English abstract).
- Liu, J.N., Feng, C.Y., Zhao, Y.M., Li, D.X., Xiao, Y., Zhou, J.H., Ma, Y.S., 2013. Characteristics of intrusive rock, metasomatism, mineralization and alteration in Yemaquan skarn Fe-Zn polymetallic deposit, Qinghai Province. *Mineral Deposits* 32, 77–93 (in Chinese with English abstract).
- Logan, M.A.V., 2000. Mineralogy and geochemistry of the Gualilán skarn deposit in the Recordillera of western Argentina. *Ore Geol. Rev.* 17, 113–138.
- Lu, H.Z., Liu, Y.M., Wang, C.L., Xu, Y.Z., Li, H.Q., 2003. Mineralization and fluid inclusion study of the Shizhuyuan W–Sn–Bi–Mo–F skarn deposit, Hunan province, China. *Econ. Geol.* 98, 955–974.
- Mao, J.W., Li, H.Y., Shimazakib, H., Raimbault, L., Guy, B., 1996. Geology and metallogeny of the Shizhuyuan skarn–greisen deposit, Hunan Province, China. *Int. Geol. Rev.* 38, 1020–1039.
- Meinert, L.D., 1982. Skarn, manto, and breccia pipe formation in sedimentary rocks of the Cananea mining district, Sonora, Mexico. *Econ. Geol.* 77, 919–949.
- Meinert, L.D., 1987. Skarn zonation and fluid evolution in the Groundhog mine, Central mining district, New Mexico. *Econ. Geol.* 82, 523–545.
- Meinert, L.D., 1992. Skarns and skarn deposits. *Geosci. Can.* 19, 145–162.
- Meinert, L.D., 1995. Compositional variation of igneous rocks associated with skarn deposits—chemical evidence for a genetic connection between petrogenesis and mineralization. *Mineralogical Association of Canada, Short Course Series* 23pp, 401–418.
- Meinert, L.D., Hefton, K.K., Mayes, D., Tasiran, I., 1997a. Application of skarn deposit zonation models to mineral exploration. *Explor. Min. Geol.* 6, 185–208.
- Meinert, L.D., Hefton, K.K., Mayes, D., Tasiran, I., 1997b. Geology, zonation, and fluid evolution of the Big Gossan Cu–Au skarn deposit, Ertsberg district, Irian Jaya. *Econ. Geol.* 92, 509–534.
- Meinert, L.D., Dippe, G.M., Nicolescu, S., 2005. World skarn deposits. *Society of Economic Geologists, Economic Geology 100th Anniversary Volume* pp, 299–336.
- Meng, F.C., Cui, M.H., Wu, X.K., Wu, J.F., Wang, J.H., 2013. Magmatic and metamorphic events recorded in granitic gneisses from the Qimantagh, East Kunlun Mountains, Northwest China. *Acta Petrol. Sin.* 29 (6), 2107–2122 (in Chinese with English abstract).
- Meng, F.C., Cui, M.H., Wu, X.K., Ren, Y.F., 2015. Heishan mafic–ultramafic rocks in the Qimantagh area of Eastern Kunlun, NW China: remnants of an early Paleozoic incipient island arc. *Gondwana Res.* 27 (2), 745–759.
- Mo, X.X., Luo, Z.H., Deng, J.F., Yu, X.H., Liu, C.D., Shen, H.W., Yuan, W.M., Liu, Y.H., 2007. Granitoids and crustal growth in the East-Kunlun orogenic belt. *Geol. J. China Univ.* 13, 403–414 (in Chinese with English abstract).
- Moecher, D.P., Chou, I.M., 1990. Experimental investigation of andradite and hedenbergite equilibria employing the hydrogen sensor technique, with revised estimates of ΔfG_m^0 at 298 for andradite and hedenbergite. *Am. Mineral.* 75, 1327–1341.
- Oyman, T., 2010. Geochemistry, mineralogy and genesis of the Ayazmant Fe–Cu skarn deposit in Ayvalik, (Balikesir), Turkey. *Ore Geol. Rev.* 37 (3), 175–201.
- Öztürk, Y.Y., Helvacı, C., 2008. Skarn alteration and Au–Cu mineralization associated with Tertiary granitoids in northwestern Turkey: evidence from the Evciler deposit, Kazdag Massif, Turkey. *Econ. Geol.* 103, 1665–1682.
- Palinkaš, S.S., Palinkaš, L.A., Renac, C., Spangenberg, J.E., Lüders, V., Molnar, F., Malíqi, G., 2013. Metallogenetic model of the Trepča Pb–Zn–Ag skarn deposit, Kosovo: evidence from fluid inclusions, rare earth elements, and stable isotope data. *Econ. Geol.* 108 (1), 135–162.
- Pan, Y.S., Zhou, W.M., Xu, R.H., Wang, D.A., Zhang, Y.Q., Xie, Y.W., Chen, T.E., Luo, H., 1996. The Early Paleozoic geological features and evolutions of the Kunlun Mountains. *Sci. China Ser. D* 26, 302–307.
- Pons, J., Franchini, M., Meinert, L., López-Escobar, L., Maydagán, L., 2010. Geology, petrography and geochemistry of igneous rocks related to mineralized skarns in the NW Neuquén basin, Argentina: implications for Cordilleran skarn exploration. *Ore Geol. Rev.* 38, 37–58.
- Qinghai Geological Survey Institute (QGSI), 2009. Potential evaluation of mineral resources in Qinghai Province—typical demonstration area report: Unpublished report, Appendix (in Chinese)
- Qinghai Regional Geological Survey Team (QRGST), 1981. Regional geological survey of BoKalikefu report: Unpublished report, Appendix (in Chinese)
- Robinson, B., Kusakabe, M., 1975. Quantitative preparation of sulphur dioxide for $^{34}\text{S}/^{32}\text{S}$ analyses from sulphides by combustion with cuprous oxide. *Anal. Chem.* 47, 1179–1181.
- Scheepers, R., 2000. Granites of the Saldania mobile belt, South Africa: radioelements and P as discriminators applied to metallogeny. *J. Geochem. Explor.* 68, 69–86.
- She, H.Q., Zhang, D.Q., Jing, X.Y., Guan, J., Zhu, H.P., Feng, C.Y., Li, D.X., 2007. Characteristics and metallogenesis of Wulanwuzhuer porphyry copper deposit in Qinghai Province. *Geol. China* 34 (2), 306–314 (in Chinese with English abstract).
- Shimazaki, H., 1980. Characteristics of skarn deposits and related acid magmatism in Japan. *Econ. Geol.* 75, 173–183.
- Shimizu, M., Iiyama, J.T., 1982. Zinc–lead skarn deposits of the Nakatatsu mine, central Japan. *Econ. Geol.* 77, 1000–1012.
- Simon, G., Kesler, S.E., Essene, E.J., Chryssoulis, S.L., 2000. Gold in porphyry copper deposits: experimental determination of the distribution of gold in the Cu–Fe–S system at 400° to 700 °C. *Econ. Geol.* 95, 259–270.
- Smith, M.P., Henderson, P., Jeffries, T.E.R., Long, J., Williams, C.T., 2004. The rare earth elements and uranium in garnets from the Beinn and Dubhaich Aureole, Skye, Scotland, UK: constraints on processes in a dynamic hydrothermal system. *J. Petrol.* 45, 457–484.
- Somarin, A.K., 2004. Garnet composition as an indicator of Cu mineralization: evidence from skarn deposits of NW Iran. *J. Geochem. Explor.* 81, 47–57.
- Somarin, A.K., Moayyed, M., 2002. Granite- and gabbronorite-associated skarn deposits of NW Iran. *Ore Geol. Rev.* 20 (3), 127–138.
- Song, Z.B., Jia, Q.Z., Zhang, Z.Y., He, S.Y., Chen, X.Y., Quan, S.C., Li, Y.Z., Zhang, Y.L., Zhang, X.F., 2010. Study on geological feature and origin of Yemaquan Fe–Cu deposit in Qimantagh Area, eastern Kunlun. *Northwest. Geol.* 34, 209–217 (in Chinese with English abstract).
- The Third Exploration Institute of Geology and Mineral Resources of Qinghai (TEIGMRQ), 2010. Mineral exploration of the Yemaquan Fe-polymetallic deposit, Golmud, Qinghai Province: Unpublished report, Appendix (in Chinese)
- Vassileva, R.D., Bonev, I.K., 2001. Manganese Amphiboles from the Skarn–Ore Pb–Zn Deposits in the Madan District. 38. Bulgarian Academy of Sciences, Central Rhodopes, Bulgaria, pp. 45–53.
- Vassileva, R.D., Bonev, I.K., 2002. Hydrothermal manganese chamosite from the vein and replacement Pb–Zn ore deposits, Madan district, Bulgaria. *Geochim. Mineral. Petrol.* 39, 81–93.
- Vassileva, R.D., Bonev, I.K., 2003. Retrograde alterations of manganese skarns in the Madan Pb–Zn deposits, South Bulgaria. *Mineral Exploration and Sustainable Development*, Millpress, Rotterdam, pp. 403–406.
- Wang, B.Z., 2011. The Study and Investigation on the Assembly and Coupling PetroTECTONIC Assemblage During Paleozoic–Mesozoic Period at Qimantagh Geological Corridor Domain PhD thesis, China Univ. Geosci, Beijing, p. 72 (in Chinese with English abstract).
- Wang, G.C., Xiang, S.Y., Garver, J.I., Wintsch, R.P., Tice, M.R., 2003. Uplift and exhumation during Mesozoic in Halaguole–Hatu area, east segment of eastern Kunlun mountains: evidence from zircon and apatite fission-track ages. *Earth Sci. J. China Univ. Geosci.* 28 (6), 645–651 (in Chinese with English abstract).
- Wang, B.Z., Luo, Z.H., Li, H.Y., Shen, H.W., Hu, X.L., 2009. PetroTECTONIC assemblages and temporal–spatial framework of the Late Paleozoic–Early Mesozoic intrusions in the Qimantagh Corridor of the East Kunlun belt. *Geol. China* 36, 769–782 (in Chinese with English abstract).
- Wang, X.L., Gao, X.P., Liu, Y.Q., Li, X.L., Zhou, X.K., Du, S.X., Cui, J.G., Dai, X.Y., Zeng, Z.C., 2010. Revision of the Qimantagh Group in west part of East Kunlun. *Northwest. Geol.* 43, 168–178 (in Chinese with English abstract).
- Wang, B.Z., Luo, Z.H., Pan, T., Song, T.Z., Xiao, P.X., Zhang, Z.Q., 2012. PetroTECTONIC assemblages and LA-ICP-MS zircon U–Pb age of Early Paleozoic volcanic rocks in Qimantagh area, Tibetan Plateau. *Geol. B. Chin.* 31, 860–874 (in Chinese with English abstract).

- Wang, Q.F., Deng, J., Li, C.S., Li, G.J., Yu, L., Qiao, L., 2014. The boundary between the Simao and Yangtze blocks and their locations in Gondwana and Rodinia: constraints from detrital and inherited zircons. *Gondwana Res.* 26 (2), 438–448.
- Wang, H., Feng, C.Y., Li, D.X., Li, C., Ding, T.Z., Liao, F.Z., 2015. Geology, geochronology and geochemistry of the Saishitang Cu deposit, East Kunlun Mountains, NW China: constraints on ore genesis and tectonic setting. *Ore Geol. Rev.* 72, 43–59.
- Williams-Jones, A.E., Samson, I.M., Ault, K.M., Gagnon, J.E., Fryer, B.J., 2010. The genesis of distal zinc skarns: evidence from the Mochito Deposit, Honduras. *Econ. Geol.* 105 (8), 1411–1440.
- Xi, R.G., Xiao, P.X., Wu, Y.Z., Dong, Z.C., Guo, L., Gao, X.F., 2010. The geological significances, composition and age of the monzonitic granite in Kendekeke iron mine. *Northwest. Geol.* 43, 195–202 (in Chinese with English abstract).
- Xiong, F.H., Ma, C.Q., Wu, L., Jiang, H.A., Liu, B., 2015. Geochemistry, zircon U-Pb ages and Sr-NdHf isotopes of an Ordovician appinitic pluton in the East Kunlun orogen: new evidence for Proto-Tethyan subduction. *J. Asian Earth Sci.* <http://dx.doi.org/10.1016/j.jseas.2015.05.025>.
- Xia, R., Wang, C.M., Deng, J., Carranza, E.J.M., Li, W.L., Qing, M., 2014. Crustal thickening prior to 220 Ma in the East Kunlun Orogenic Belt: insights from the Late Triassic granitoids in the Xiao-Nuomuhong pluton. *J. Asian Earth Sci.* 93, 193–210.
- Xiao, Y., Feng, C.Y., Liu, J.N., Yu, M., Zhou, J.H., Li, D.X., Zhao, Y.M., 2013. LA-MC-ICP-MS zircon U-Pb dating and sulfur isotope characteristics of Kendekeke Fe – polymetallic deposit, Qinghai Province. *Mineral Deposits* 32, 177–186 (in Chinese with English abstract).
- Xiong, F.H., Ma, C.Q., Jiang, H.A., Liu, B., Zhang, J.Y., Zhou, Q., 2013. Petrogenetic and tectonic significance of Permian calc-alkaline lamprophyres, East Kunlun orogenic belt, Northern Qinghai – Tibet Plateau. *Int. Geol. Rev.* 55 (14), 1817–1834.
- Xu, Z.Q., Jiang, M., Yang, J.S., 1996. Tectonophysical process at depth for the uplift of the northern part of the Qinghai–Tibet Plateau: illustrated by the geological and geophysical comprehensive profile from Golmud to the Tanggula Mountains, Qinghai Province, China. *Acta Geol. Sin.* 70, 195–206 (in Chinese with English abstract).
- Xu, T., Wu, Z.B., Zhang, Z.J., Tian, X.B., Deng, Y.F., Wu, C.L., Teng, J.W., 2014. Crustal structure across the Kunlun fault from passive source seismic profiling in East Tibet. *Tectonophysics* 627, 98–107.
- Yang, J.S., Robinson, P.T., Jiang, C.F., Xu, Z.Q., 1996. Ophiolites of the Kunlun mountains, China and their tectonic implications. *Tectonophysics* 258, 215–231.
- Yin, A., Harrison, T.M., 2000. Geologic evolution of the Himalayan–Tibetan orogen. *Ann. Rev. Earth Planet. Sci.* 28, 211–280.
- Yin, H.F., Zhang, K.X., 1997. Characteristics of the Eastern Kunlun Orogenic belt. *Earth Sci. J. China Univ. Geosci.* 22, 339–342 (in Chinese with English abstract).
- Yuan, W.M., Dong, J., Wang, S.C., Carter, A., 2006. Apatite fission track evidence for Neogene uplift in the eastern Kunlun Mountains, northern Qinghai–Tibet Plateau, China. *J. Asian Earth Sci.* 27 (6), 847–856.
- Zhai, D.G., Liu, J.J., Zhang, H.Y., Wang, J.P., Jian, P., Su, L., Yang, X.A., Wu, S.H., 2013. Origin of oscillatory zoned garnets from the Xieertala Fe–Zn skarn deposit, northern China: in situ LA-ICP-MS evidence. *Lithos* 190, 279–291.
- Zhang, A.K., 2012. Studies on Late Paleozoic–Early Mesozoic Magmatism and Mineralization in Yemaquan Area, Qinghai Province PhD thesis, China Univ. Geosci, Beijing, pp. 19–101 (in Chinese with English abstract).
- Zhang, K.X., Zhu, Y.H., Yin, H.F., 2004. Application of tectonic facies in geological mapping in East Kunlun orogenic belt. *Earth Sci. J. China Univ. Geosci.* 29, 661–666 (in Chinese with English abstract).
- Zhao, Y.M., 1997. Metasomatic zoning in some major Pb–Zn-polymetallic skarn deposits of China. *Mineral Deposits* 16, 120–129 (in Chinese with English abstract).
- Zhao, Y.M., Tan, H.J., Xu, Z.N., Yuan, R.G., Bi, C.E., Zheng, R.L., Li, D.X., Sun, J.H., 1983. Chinese Academy of Geological Sciences, Mineral Resource and Geology Institute, Special Issue 1 pp. 1–141 (in Chinese).
- Zhao, Y.M., Zhang, Y.N., Lin, W.W., 1997. Characteristics of pyroxenes and pyroxenoids in skarn deposits of China and their relationship with metallization. *Mineral Deposits* 16, 318–329 (in Chinese with English abstract).
- Zhao, Y.M., Li, D.X., Dong, Y.G., 2002. Further discussion on Pb–Zn–Ag-bearing manganese skarn formation. *Mineral Deposits* 21 (z3), 548–552 (in Chinese).
- Zhao, Y.M., Dong, Y., Li, D., Bi, C., 2003. Geology, mineralogy, geochemistry, and zonation of the Bajiazi dolostone-hosted Zn–Pb–Ag skarn deposit, Liaoning Province, China. *Ore Geol. Rev.* 23, 153–182.
- Zhao, Y.M., Feng, C.Y., Li, D.X., Liu, J.N., Xiao, Y., Yu, M., Ma, S.C., 2013. Metallogenetic setting and mineralization-alteration characteristics of major skarn Fe-polymetallic deposits in Qimantagh area, western Qinghai Province. *Mineral Deposits* 32, 1–19 (in Chinese with English abstract).
- Zharikov, V.A., 1970. Skarns. *Int. Geol. Rev.* 12, 541–559 (619–647 and 760–775.).
- Zheng, X.R., 1983. Calculation of the Fe^{3+} and Fe^{2+} contents in silicate and Ti–Fe oxide minerals from EPMA data. *Acta Mineral. Sin.* 1, 55–62 (in Chinese with English abstract).